Construction of approximate invariants for nonintegrable Hamiltonian systems

Yongjun Li,[1,*] Derong Xu,[1] and Yue Hao[2]

[1]*Brookhaven National Laboratory, Upton, New York 11973, USA*
[2]*Michigan State University, East Lansing, Michigan 48864, USA*

(Received 21 January 2025; accepted 2 July 2025; published 28 July 2025)

We present a method to construct high-order polynomial approximate invariants (AI) for nonintegrable Hamiltonian dynamical systems and apply it to a modern ring-based particle accelerator. Taking advantage of a special property of one-turn transformation maps expressed as square matrices, AIs can be constructed order by order iteratively. Evaluating AI with simulation data, we observe that AI's fluctuation is actually a measure of chaos. Through minimizing the fluctuations, the stable region of long-term motions, i.e., the dynamic aperture of the accelerator, could be enlarged.

DOI: 10.1103/m349-wmnr

I. INTRODUCTION

The construction of the invariant phase-space tori of Hamiltonian systems is important in many mathematical physics fields (see Refs. [1–8] and references therein). For nonintegrable Hamiltonian systems, exact solutions for motion are often impossible. They generally lack sufficient conserved quantities. However, Kolmogorov-Arnold-Moser theory [9] proves that approximate invariants (AI) could still exist in such systems. The theory addresses the stability of motion in near-integrable Hamiltonian systems that can be seen as small perturbations of integrable systems. If the perturbation is small enough, a significant portion of the invariant tori of the integrable system survives, though deformed. These surviving tori act as quasi-invariants or AIs, where the motion remains confined and quasiperiodic, preserving the structure of the integrable case. Even though resonances can disrupt some tori, many tori persist in a "cantorized" form, as long as certain nonresonance conditions are met. The remnants of the AI tori provide a structure that partially resists chaotic diffusion, preserving long-term stability in certain regions of phase space. Such a region is also known as "dynamic aperture (DA)" in particle accelerator physics [10]. A sufficient DA is often required for beam manipulation and machine operation. It is important to explicitly obtain the AIs of given lattices and evaluate their fluctuations when designing and optimizing modern accelerator magnetic lattices [1,2].

II. METHOD

The evolution of motion in a periodical Hamiltonian system can be approximately represented with polynomial maps. These maps can be extracted with the truncated power series algorithm [11–13] to any arbitrary order. For example, consider a four-dimensional phase-space vector $[x, p_x, y, p_y]^T$, which represents an on-momentum charged particle's motion in the transverse plane in an accelerator. The superscript ^{T} represents the transpose of matrices or vectors. First, we construct a Ω-th order vector

$$Z = [x, p_x, y, p_y, x^2, xp_x, xy, xp_y, p_x^2, p_xy, \ldots, p_y^{\Omega}]^T. \quad (1)$$

Let the one-turn map of the system be written in a matrix form as

$$Z_{\text{final}} = MZ_{\text{initial}}, \quad (2)$$

where M is a square matrix. Such a map is usually nonsymplectic due to the truncation of higher-order polynomial terms. Following the method in Chao's note [14], an Ω-order Taylor series approximate invariant W can be written as

$$W^{(\Omega)} = V^T Z, \quad (3)$$

with V as the coefficient vector yet to be found. Since W is an invariant, for any Z after one-turn transformation through M, we have

$$V^T Z = V^T MZ \Longrightarrow V = M^T V. \quad (4)$$

*Contact author: yli@bnl.gov

Published by the American Physical Society under the terms of the Creative Commons Attribution 4.0 International license. Further distribution of this work must maintain attribution to the author(s) and the published article's title, journal citation, and DOI.

It means that the vector V needs to be M^T's eigenvector with its eigenvalue as 1. However, when applying a direct eigenanalysis on the $\Omega(\geq 3)$-order matrix M^T, it usually fails to yield proper AIs. It is because the coefficients of higher orders in M^T are significantly greater than the lower orders. More specifically, the magnitude incremental step at each nth order is $n!$. Therefore, the highest order terms dominate the eigenanalysis, and the obtained eigenvectors usually have near to zero coefficients in the low order terms. It might yield multiple but independent eigenvectors. To overcome this difficulty, we introduce a method to start with the well-known linear Wronskian invariants (also known as Courant-Snyder invariants [15] for uncoupled linear motion) and then iteratively construct higher-order AIs by taking advantage of the special property of the square matrix. In this paper, the National Synchrotron Light Source II (NSLS-II) storage ring [16] is used as a real-world example for illustration. Its fifth one-turn square matrix M is constructed by sequentially concatenated the magnetic elements as shown in Fig. 1. M^T matrix is a sparse matrix, with its elements in the top-right blocks being 0's, because any nth order term in Z must be a function of the same and even-higher orders terms ($\geq n$th), but not of the lower order terms ($<n$th), i.e.,

$$Z^n_{\text{final}} = \sum_{i\geq n} m_i Z^i_{\text{initial}} \tag{5}$$

This property actually enables us to construct AIs order-by-order iteratively.

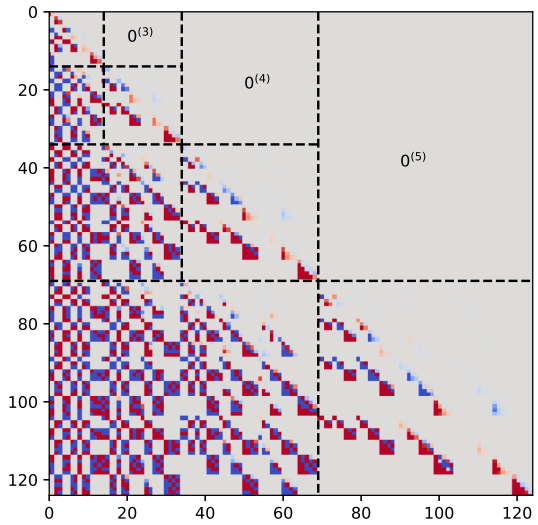


FIG. 1. Up to fifth-order blocked square matrix M^T. The first top-left 14×14 block is used to construct linear AIs $W^{(2)}_{1,2}$. Then the expanded 34×34, 69×69 and $125\times 125,\cdots$ square matrices are used to obtain high-order AIs $W^{(3,4,5,\ldots)}_{1,2}$ respectively, and so on. Note that all elements in the top-right blocks ($0^{(3-5)}$) are 0's.

We start with the linear invariants, then construct higher-order AIs on top of them. Even in the linear case, Z must be kept up to the quadratic terms in order to find two quadratic invariants $W^{(2)}_{1,2}$. Here superscript $^{(2)}$ indicates the order of W, and subscripts $_{1,2}$ are their indices. First, a 14×14 square matrix M^T truncated up to the quadratic terms is used. The eigenanalysis on M^T yields two eigenvectors $V^{(2)}_{1,2}$ with their eigenvalues as 1:

$V^{(2)}_1$		$V^{(2)}_2$	
2000	4.883952×10^{-2}	0020	2.969949×10^{-1}
0200	2.047522×10^{1}	0002	3.367061×10^{0}

Here each monomial is represented with the first four integers as the power indices of x, p_x, y, p_y, and the last float as its coefficient. These two invariants can be easily recognized as the Courant-Snyder invariants in the horizontal and vertical planes, respectively, $W_{u=x,y} = \gamma_u u^2 + 2\alpha_u u p_u + \beta_u p_u^2$, with the Twiss parameters α, β, γ. The disappearance of two crossing terms xp_x and yp_y is simply due to the local $\alpha_{x,y} = 0$.

Next, we construct cubic AIs by adding some additional cubic terms into linear invariants $V = [V^{(2)}, V^{(3)}]$, where $V^{(3)}$ represents the cubic coefficients yet to be found. By observing the form of the cubic square matrix M^T (34×34) in Fig. 1, we notice that its upright blocks $0^{(3)}$ are composed of 0's; therefore, it can be divided into 4 submatrices $M^T = \left[\begin{smallmatrix} m_0 & 0^{(3)} \\ m_2 & m_3 \end{smallmatrix}\right]$. Here m_0 with a dimension (14×14) is the quadratic matrix already being analyzed previously, $0^{(3)}$ (14×20) is a zero matrix, m_2 (20×14) and m_3 (20×20) are two matrices with the cubic term coefficients. The new cubic AIs need to satisfy the following condition:

$$\begin{bmatrix} V^{(2)} \\ V^{(3)} \end{bmatrix} = \begin{bmatrix} m_0 & 0^{(3)} \\ m_2 & m_3 \end{bmatrix} \begin{bmatrix} V^{(2)} \\ V^{(3)} \end{bmatrix}. \tag{6}$$

Because the first row in Eq. (6) is already valid automatically, the cubic term coefficient $V^{(3)}$ can be simply solved with

$$V^{(3)} = (I - m_3)^{-1} m_2 V^{(2)}. \tag{7}$$

By solving Eq. (7), the cubic terms in two AIs are obtained as

$V^{(3)}_1$		$V^{(3)}_2$	
3000	1.327349×10^{-1}	1020	-4.703005×10^{0}
2100	-6.078392×10^{-1}	1011	-1.778960×10^{0}
⋯	⋯		
0102	4.370392×10^{1}	0102	-5.597472×10^{1}

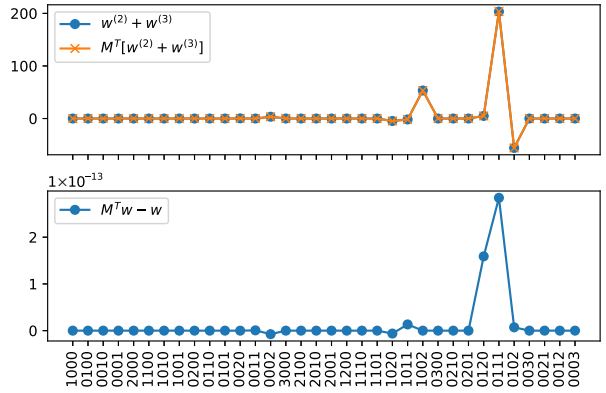


FIG. 2. Comparison a third-order AI's coefficient $[V^{(2)}+V^{(3)}]$ with its one-turn transformation $M^T[V^{(2)}+V^{(3)}]$. Top: the values of all 34 monomial coefficients. Bottom: the difference between them represents the quality of the AI.

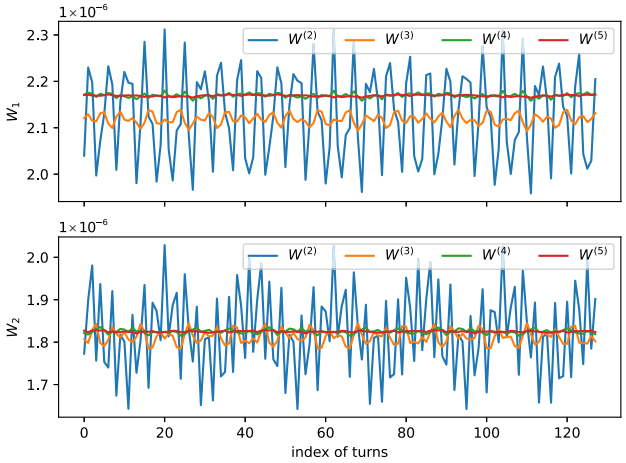


FIG. 3. Fluctuations of two AIs $W_{1,2}^{(2,3,4,5)}$ at different orders (2nd–5th) by evaluating with a simulated trajectory.

The constructed cubic AI's coefficients $[V^{(2)},V^{(3)}]^T$ can be compared with its one-turn transformation $M^T[V^{(2)},V^{(3)}]^T$ as shown in Fig. 2. The maximum difference of coefficients is around 3×10^{-13}. It is worthwhile to mention that the existence of the solution in Eq. (7) requires the square matrix $(I-m_3)$ to be invertible. In some cases, this condition might not be satisfied, which means the appearance of broken tori [14] due to a third resonance. However, for most stable systems, such as particle accelerators, their $(I-m_3)$ usually invertible because their fundamental frequency is intentionally chosen to be off resonant. Once the cubic AIs are obtained, we can iteratively apply Eq. (6) to obtain even higher-order AIs.

III. APPLICATION IN LATTICE DESIGN

Once the AIs are obtained, we can verify them with simulation data. Here a simulated 128 turns trajectory starting with an initial condition $x=6.4\,\text{mm}, y=2.6\,\text{mm}$, $p_{x,y}=0$ is obtained with a symplectic tracking algorithm [17]. After evaluating different order AIs $W_{1,2}^{(2,3,4,5)}$ with the simulated data, they are observed converging gradually with reduced fluctuations as illustrated in Fig. 3, which indicates the accuracy of AIs is improved by including more higher-order terms. However, the AIs' quality becomes worse when their order Ω is above 5 in this specific example. Thus far, it is unclear if the higher-order AIs are spoiled by the accumulated numerical errors or if they simply do not exist at all.

As seen in Fig. 3, these AIs are only approximately constant, rather than exactly. After evaluating with simulated data, AI's fluctuation increases gradually with oscillation amplitude as shown in Fig. 4. The fluctuations of linear AIs (also known as "the action smear") are traditionally used as a chaos indicator in accelerator physics [18]. Once the fluctuations exceed a certain threshold, the approximate tori break down and stable particle motion can no longer be maintained.

There exist many other chaos indicators (some of them are compared in Refs. [19,20]), which can be used for studying nonlinear beam dynamics. Among them, the frequency map analysis (FMA) [21,22], Shannon entropy [23], forward-reversal integration [24–26] are selected to compare with the fluctuation of AIs for the NSLS-II ring in Fig. 5. Here the relative AIs' fluctuation is defined as $\frac{\sigma_{W_1}}{|\langle W_1\rangle|}+\frac{\sigma_{W_2}}{|\langle W_2\rangle|}\cdot\sigma_{W_{1,2}}$ represent the standard deviations of multiple-turn W's, and $|\langle W_{1,2}\rangle|$ are their absolute mean values. In Fig. 5, various chaos indicators display a common pattern, in which regular motions gradually dilute into chaos with amplitude. Note that the color scales used in these four cases are not directly comparable, because of the different chaos metrics used. From the comparison, we observe that the FMA excels at detecting resonances, which needs a spectral analysis, such as FFT or NAFF.

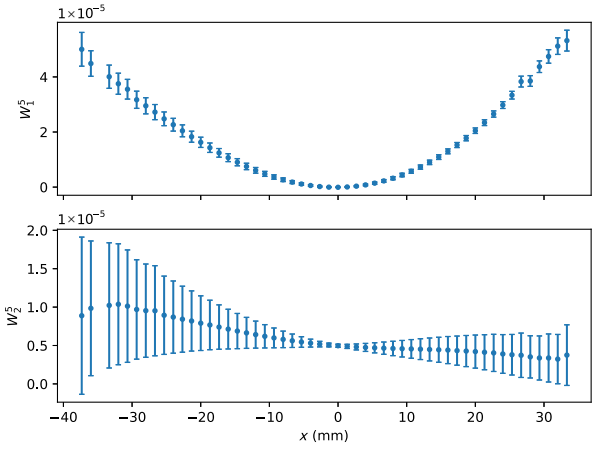


FIG. 4. Absolute fluctuations of the fifth-order AIs with the horizontal oscillation amplitude (the initial vertical amplitude is 6 mm) in the NSLS-II ring.

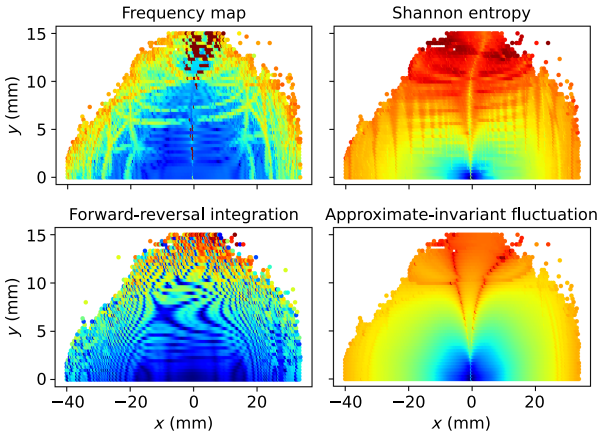


FIG. 5. Comparison of different chaos indicators for the NSLS-II ring. Top left: frequency map analysis; top right: Shannon entropy; bottom-left: forward-reversal integration; bottom right: fluctuations of approximate invariant. They display a common pattern, in which regular motions gradually dilute into chaos with the amplitude.

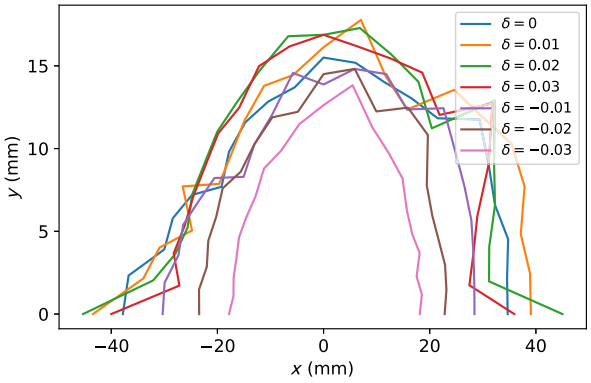


FIG. 6. On- and off-momentum dynamic apertures for the optimal solution obtained by minimizing the fluctuations of AIs. Here $\delta = \frac{\Delta P}{P}$ represents charged particle's relative momentum deviations.

Such spectral analysis is also adopted in Ref. [7]. The forward-reversal integration mainly describes the unpredictability of long-term motions, relying on the randomness in computation. The Shannon entropy and AI's fluctuations are actually similar. Both describe the fluctuations of predefined motion constants. While computing Shannon entropy, the phase-space region needs to be discretized into a mesh grid, which makes the transition from regular motion to chaos not as smooth as AI. While AI has an explicit function form, the characterization of chaos is more accurate.

In designing accelerators, it is generally believed that, by suppressing the chaos of beam motions, their dynamic apertures can be enlarged. Since AI's fluctuations are a measure of chaos, we explore the possibility of optimizing the NSLS-II magnetic lattice by suppressing the fluctuations of its fifth-order AIs. Technically, by tuning some harmonic sextupoles, we aim to minimize the AI's fluctuations on a specific trajectory starting with a given initial condition $x = 15.7$ mm, $y = 3.7$ mm, $p_{x,y} = 0$. Once the optimal sextupole configuration is reached, the on- and off-momentum dynamic apertures are obtained by tracking particles for 2048 turns with the simulation code ELEGANT [27] and illustrated in Fig. 6. More detailed simulations confirm that this nonlinear lattice performance is similar to our baseline design [16]. However, the suppression of AI's fluctuation is more efficient than other multiparticle tracking-based optimizations, such as [28,29]. The optimization is accomplished within several hours, even on a single core computer.

It is worth mentioning another method to construct approximate actions also from a square matrix, as described in Ref. [7]. Its square matrix is constructed but with the monomials of the phase -space variables $z = \bar{x} - i\bar{p}$ after applying the Courant-Snyder parameterization. Then, a Jordan analysis is carried out to determine the amplitude-dependent-tune shift and the approximate actions W_0. Predicting the long-term stability of each initial condition in phase space requires an additional transformation from the approximate action-angle pair to a rigid rotation, achieved through an iterative process in the frequency domain. Mathematically, such a Jordan decomposition is a block-diagonal matrix with Jordan blocks. Reference [7] further explains a method of detecting resonances, including high-order weak ones, which demands substantial computational resources such as high-dimensional Fourier analysis. Alternatively, our proposed method utilizes the eigenanalysis on the raw square matrix (without the Courant-Snyder parameterization). It aims to find a diagonal matrix (or one as close to diagonal as possible) that is similar to the original matrix, thereby significantly reducing the required computational effort. However, the most valuable information, i.e., the approximate invariants, is constructed explicitly. With the obtained AIs, other tune related information, such as the tune shift with amplitude, can be further derived using the methods explained in Refs. [30,31].

IV. CONCLUSION

In summary, we present a method to construct the approximate invariants of nonintegrable Hamiltonian systems and demonstrate its application on a modern accelerator. We also demonstrate that the fluctuation of AIs, when evaluated with simulation data, serves as a chaos indicator and can be potentially used as an efficient optimization objective in designing modern accelerators.

ACKNOWLEDGMENTS

We would like to thank S. Nagaitsev (BNL) and C. Mitchell (LBNL) for their valuable discussion and constructive suggestion, P. Belanger and G. Sterbini (CERN) for a detailed numerical comparison and confirmation, H. Zhang (JLab), Y. Hidaka, and D. Hidas (BNL)

for their consistent supports in computation. This research is supported by the U.S. Department of Energy (DOE) under Contract No. DE-SC0012704, Office of Basic Energy Sciences, Field Work Proposal 2025-BNL-PS040, and the DOE HEP Award No. DE-SC0019403. The co-author D. X. is supported by the DOE early career award.

DATA AVAILABILITY

The data are not publicly available. The data are available from the authors upon reasonable request.

[1] J. Hagel, Invariants of betatron motion and dynamic aperture: An analytic approach, Technical Report No. LEP-TH/86-22, CERN, 1986.

[2] Robert L. Warnock, Close approximations to invariant tori in nonlinear mechanics, Phys. Rev. Lett. **66**, 1803 (1991).

[3] Mikko Kaasalainen and James Binney, Construction of invariant tori and integrable Hamiltonians, Phys. Rev. Lett. **73**, 2377 (1994).

[4] Mikko Kaasalainen, Construction of invariant tori in chaotic regions, Phys. Rev. E **52**, 1193 (1995).

[5] Alessandra Celletti, Antonio Giorgilli, and Ugo Locatelli, Improved estimates on the existence of invariant tori for Hamiltonian systems, Nonlinearity **13**, 397 (2000).

[6] Teemu Laakso and Mikko Kaasalainen, Canonical methods of constructing invariant tori by phase–space sampling, Physica (Amsterdam) **243D**, 14 (2013).

[7] Li Hua Yu, Analysis of nonlinear dynamics by square matrix method, Phys. Rev. Accel. Beams **20**, 034001 (2017).

[8] Philippe Belanger and Guido Sterbini, Numerical evaluation of the integrals of motion in particle accelerator tracking codes, arXiv:2503.19122.

[9] Rafael De la Llave *et al.*, A tutorial on KAM theory, in *Proceedings of Symposia in Pure Mathematics* (Citeseer, 2001), Vol. 69, pp. 175–296, https://www.dancenet. org/images/files/events/rtns2008/materiales/notes_de_la_llave .pdf.

[10] Alexander Wu Chao, Maury Tigner, Hans Weise, and Frank Zimmermann, *Handbook of Accelerator Physics and Engineering* (World Scientific, Singapore, 2003), Chap. 2.3.7.

[11] Martin Berz, Modern map methods for charged particle optics, Nucl. Instrum. Methods Phys. Res., Sect. A **363**, 100 (1995).

[12] Lingyun Yang, Array based truncated power series package, in *Proceedings of the International Particle Accelerator Conference (ICAP'09), San Francisco, CA* (2009), pp. 371–373, https://accelconf.web.cern.ch/ICAP2009/papers/thpsc059.pdf.

[13] He Zhang, CppTPSA/pyTPSA: A C++/Python package for truncated power series algebra, J. Open Source Software **9**, 4818 (2024).

[14] Alexander Wu Chao, *Lectures on Accelerator Physics* (World Scientific, Singapore, 2020).

[15] Ernest D. Courant and Hartland S. Snyder, Theory of the alternating-gradient synchrotron, Ann. Phys. (N.Y.) **3**, 1 (1958).

[16] Steve Dierker, NSLS-II preliminary design report, Brookhaven National Laboratory, Report No. BNL-94744-2007, 2007, 10.2172/1010602.

[17] Haruo Yoshida, Construction of higher order symplectic integrators, Phys. Lett. A **150**, 262 (1990).

[18] A. Chao, D. Johnson, S. Peggs, J. Peterson, C. Saltmarsh, L. Schachinger, R. Meller, R. Siemann, R. Talman, P. Morton *et al.*, Experimental investigation of nonlinear dynamics in the Fermilab Tevatron, Phys. Rev. Lett. **61**, 2752 (1988).

[19] A. Bazzani, M. Giovannozzi, C. E. Montanari, and G. Turchetti, Performance analysis of indicators of chaos for nonlinear dynamical systems, Phys. Rev. E **107**, 064209 (2023).

[20] C. E. Montanari, R. B. Appleby, A. Bazzani, M. Giovannozzi, S. Redaelli, G. Sterbini, and G. Turchetti, Chaos indicators for non-linear dynamics in circular particle accelerators, arXiv:2504.12741.

[21] Jacques Laskar, Frequency map analysis and particle accelerators, in *Proceedings of the 2003 Particle Accelerator Conference* (IEEE, New York, 2003), Vol. 1, pp. 378–382.

[22] Yannis Papaphilippou, Detecting chaos in particle accelerators through the frequency map analysis method, Chaos **24**, 024412 (2014).

[23] Yongjun Li, Kelly Anderson, Derong Xu, Yue Hao, Kiman Ha, Yoshiteru Hidaka, Minghao Song, Robert Rainer, Victor Smaluk, and Timur Shaftan, Online regularization of Poincaré map of storage rings with Shannon entropy, Phys. Rev. Accel. Beams **28**, 034001 (2025).

[24] Kilean Hwang, Chad Mitchell, and Robert Ryne, Rapidly converging chaos indicator for studying dynamic aperture in a storage ring with space charge, Phys. Rev. Accel. Beams **23**, 084601 (2020).

[25] Yongjun Li, Yue Hao, Kilean Hwang, Robert Rainer, An He, and Ao Liu, Fast dynamic aperture optimization with forward-reversal integration, Nucl. Instrum. Methods Phys. Res., Sect. A **988**, 164936 (2021).

[26] Federico Panichi, Krzyszof Goździewski, and Giorgio Turchetti, The reversibility error method (REM): A new, dynamical fast indicator for planetary dynamics, Mon. Not. R. Astron. Soc. **468**, 469 (2017).

[27] Michael Borland, ELEGANT: A flexible SDDS-compliant code for accelerator simulation, Argonne National Laboratory, IL, Technical Report No. LS-287; No. TRN: US0004540, 2000, 10.2172/761286.

[28] Lingyun Yang, Yongjun Li, Weiming Guo, and Samuel Krinsky, Multiobjective optimization of dynamic aperture, Phys. Rev. ST Accel. Beams **14**, 054001 (2011).

[29] Yongjun Li, Weixing Cheng, Li Hua Yu, and Robert Rainer, Genetic algorithm enhanced by machine learning in dynamic aperture optimization, Phys. Rev. Accel. Beams **21**, 054601 (2018).

[30] Sergei Nagaitsev and Timofey Zolkin, Betatron frequency and the Poincaré rotation number, Phys. Rev. Accel. Beams **23**, 054001 (2020).

[31] Chad E. Mitchell, Robert D. Ryne, Kilean Hwang, Sergei Nagaitsev, and Timofey Zolkin, Extracting dynamical frequencies from invariants of motion in finite-dimensional nonlinear integrable systems, Phys. Rev. E **103**, 062216 (2021).